PHYSICAL REVIEW B VOLUME 6, NUMBER 6 15 SEPTEMBER 1972

Self-Consistent Electronic Structure of Solid Surfaces

J. A. Appelbaum and D. R. Hamann
Bell Laboratories, Murray Hill, New Jersey 07974
(Received 23 May 1972)

We have developed a method for calculating electron states in the surface region of a semi-infinite solid taking full account of the three-dimensional nature of the lattice potential. The Schrödinger equation is integrated numerically in a region consisting of the last few atomic layers and the vacuum, and optimally matched to a linear combination of Bloch (pseudo) wave functions in the interior. The potential in the surface region is computed self-consistently from the valence-charge density by solving Poisson's equation, using a local approximation to the exchange and correlation contribution, and representing the cores by a model potential. As an illustration of the practical applicability of the method, the electronic structure of the (100) surface of Na has been calculated.

I. INTRODUCTION

Over the past few decades there has been an enormous advance in the understanding of the electronic structure of bulk solids. Comparable developments in the theory of solid-vacuum interfaces have been hampered for two main reasons: First, the loss of three-dimensional periodicity associated with the formation of the surface introduces additional theoretical complexities. Second, the lack of a significant accumulation of reproducible experimental data bearing on the surface electronic structure until the last few years has inhibited attempts at overcoming the formidable theoretical difficulties.

Theoretical attempts to characterize the surface region can be divided into two general classes. In the first, the periodic potential of the bulk is assumed to persist undisturbed up to a plane at which it is abruptly terminated and replaced by a constant potential representing the vacuum. This model has been frequently applied in the calculation of bound surface states.[1] The difficulty with this approach is that the actual potential smoothly rises from its bulk structure to its vacuum value. The way it does so may well play an important role in determining the existence and the energy of these surface states, as well as determining how the valence electrons capable of participating in chemisorption protrude into the vacuum. The abrupt approximation has also been widely used in the calculation of low-energy-electron-diffraction (LEED) intensities.[2] In this case the approximation might be expected to have greater validity since, unlike the case of the valence electrons, the LEED electrons are primarily sensitive to the potentials in the ionic cores, which may be presumed to be unchanged by proximity to the surface.

In the second general class of approaches, the main emphasis is placed on being able to calculate the potential connecting the bulk with the vacuum. In doing so, the three-dimensional lattice of ions is replaced by a uniform abruptly terminated distribution of positive charge. The electronic charge distribution and the potential are then self-consistently obtained.[3,4] This "jellium" model is a reasonable first approximation for those metals which are known to be free-electron-like in the bulk. There are, however, many limitations on the applicability of this model. It is conceptually unsuitable for use with semiconductors, and leads to serious quantitative errors when applied to noble and transition metals.[4] The model fails to distinguish the properties of various crystal faces, which are known to vary significantly even for those metals to which it is a reasonable first approximation.

There have been a few attempts to incorporate the discrete lattice potential into the self-consistent calculation of the surface potential. The earliest of these, due to Smoluchowski,[5] considered the positive charge to be uniformly distributed in Wigner-Seitz cells, giving a jellium interior with a corrugated face. He assessed the trends in work function dependence on crystal-face structure primarily by assuming that the electron density was smooth parallel to the surface and terminated abruptly. He also considered the effects of allowing the electron density to relax to an equilibrium distribution determined by minimizing the Weizsäker formula for the electron energy as a functional of the density.[6] More recently, Smith used a similar model for the positive charge and a more sophisticated energy functional to calculate the work function of the tungsten 111 face.[7] He did not, however, permit the electron density to vary parallel to the surface.

Perhaps the most successful attempt to date to include the effects of the lattice on surface properties was carried out by Kohn and Lang.[4] Starting with a self-consistent quantum-mechanical solution for the jellium model, they rigorously calcu-

lated the first-order contributions of the lattice pseudopotential to the surface energy and the work function for a large number of metals. A nonperturbational study of the influence of the lattice was carried out by Bennett and Duke[8] using a one-dimensional Kronig-Penney model for the lattice potential. Some of the difficulties entailed in carrying out a three-dimensional quantum-mechanical calculation have been discussed by Boudreaux.[9] He suggests a dielectric formulation for the potential, but does not present a prescription for calculating wave functions which satisfy the relevant boundary conditions.

The object of this paper is to present a tractable procedure for carrying out self-consistent quantum-mechanical calculations in which the three-dimensional lattice is included nonperturbationally, and illustrate its application.[10] The procedure treats the semi-infinite solid, which we believe to be the most effective model for isolating the properties of the surface.

Any such calculation has as its major tasks the determination of the potential and the calculation of the occupied wave functions. The potential of the solid loses its three-dimensional periodicity as we pass from deep in the bulk into the surface region. This is a combined result of several effects. First of all, we are dealing with a semi-infinite rather than an infinite lattice. Even if the bulk electronic distribution extended unmodified up to the surface plane, the long range of the Coulomb interaction would cause the potential to lose its periodicity in the normal direction. In addition, we expect important modifications of the electronic charge density in the surface region. These are expected to occur primarily in the valence charge. In most cases the core electrons will be sufficiently tightly bound that they will undergo essentially no modification in the surface region. This leads us to approximate the contribution of the ionic cores to the potential as a superposition of identical model potentials which are adjusted to fit empirically determined bulk pseudopotential parameters.[11] We calculate the valence-electron contribution self-consistently, using a local approximation for exchange and correlation.

Once a starting approximation to the potential is arrived at, the occupied wave functions must be obtained from the solution of the Schrödinger equation. A key step in the calculation is to choose a plane parallel to the surface such that to the left the solid is indistinguishable from the bulk. Such a choice can always be made consistent with the degree of over-all accuracy one desires. In the bulk solid, the solutions are appropriate linear combinations of degenerate Bloch functions. These must smoothly join solutions of the wave equation in the region to the right of the plane, where the potential is different from the bulk. In this "surface region," the wave functions retain periodic symmetry in the parallel direction. We have chosen to calculate these using the Laue representation,[12] in which a Fourier expansion in the parallel coordinates is combined with the coordinate representation in the normal direction.

To obtain the valence-electron charge density, wave functions must be calculated corresponding to a mesh of points in the occupied portions of the bulk Brillouin zone. This charge density is used to find a new potential in the surface region, and this procedure is iterated to self-consistency.

As an illustration of the procedure outlined above, we have carried out a calculation of the electronic structure of the (100) surface of sodium.

The remainder of the paper is organized as follows: The wave-function calculation is described in detail in Sec. II, and the potential calculation in Sec. III. A discussion of the sodium surface calculation will be given in Sec. IV. The general applicability of the method to a broad range of problems will be considered in the concluding section V.

II. WAVE-FUNCTION CALCULATION

In this section, we will assume that the (pseudo) potential in the bulk and in the surface region is given. The bulk potential is characterized by its Fourier components $V_{\vec{G}}$, where $\vec{G}$ is a reciprocal-lattice vector. Taking z as the surface-normal direction, the surface-region potential is characterized by the set of functions $V_{\vec{G}_{\parallel}}(z)$, where $\vec{G}_{\parallel}$ is the projection of $\vec{G}$ on the surface plane.

The wave functions we wish to calculate are scattering states specified by choosing a particular Bloch wave $\psi_{\vec{k}}(\vec{x})$ to be incident from deep in the bulk (we suppress the band index). The asymptotic form of the wave then consists of the incident wave plus one or more reflected Bloch waves in the bulk, and for the case of valence electrons no transmitted wave in the vacuum. This formulation is pictured schematically in Fig. 1. The reflected waves have wave vectors $\vec{k}'$, with $\vec{k}'_{\parallel}=\vec{k}_{\parallel}$, and one of them must have the same band index as the incident wave. This wave will have $k'_z=-k_z$. If states from other bands are degenerate with the incident wave, these will also occur in the reflected set, and their k_z components must be found from the band structure. We will ignore this possibility for present purposes, since the generalization of the single reflected wave case to that of several reflected waves is simple. The incident and reflected Bloch waves are expressed as Fourier series,

$$\psi_{\vec{k}}(\vec{x})=\sum_{\vec{G}}\psi_{\vec{G}}\,e^{i(\vec{k}-\vec{G})\cdot\vec{x}}, \tag{2.1}$$

where the set of G's to be included in the sum is

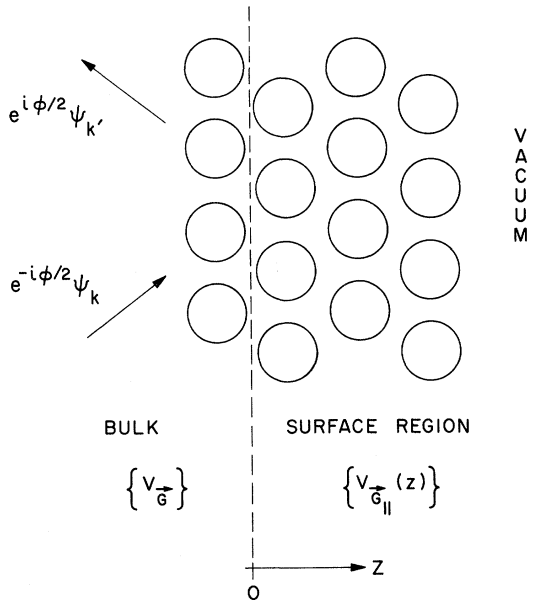

FIG. 1. Schematic representation of the vicinity of a solid surface indicating the key elements of our treatment. A plane shown by the dashed line separates the bulk, where the potential is fully periodic and represented by its reciprocal-lattice components $V_{\vec{G}}$, from the surface region. Here only two-dimensional periodicity is assumed and the potential is expanded with arbitrary functional form in the z direction for each component $V_{G_\parallel}(z)$. Incident and reflected Bloch waves $\psi_{\vec{K}}$ and $\psi_{\vec{K}'}$ are superposed with phase shift φ and joined to a numerically integrated solution at $z=0$.

selected to give a representation of the wave function which is adequate for the desired accuracy. This selection must be handled on a case-by-case basis, and has been widely discussed in the band-structure literature. Since we intend to deal with pseudopotentials and pseudo-wave-functions, the set should not be too large. Given $V_{\vec{G}}$ and the chosen basis set, the first step in the computation is to find $E(\vec{k})$ and the coefficients $\psi_{\vec{G}}$ by a standard matrix eigenvalue calculation. Components of the reflected wave are easily found from those of the incident wave.

The wave function in the surface region can be expanded as

$$u(\vec{x})=\sum_{\vec{G}_\parallel} u_{\vec{G}_\parallel}(z)\, e^{i(\vec{k}_\parallel-\vec{G}_\parallel)\cdot\vec{x}}\,, \tag{2.2}$$

where for consistency the set of $\vec{G}_\parallel$ must comprise the parallel components of the set of $\vec{G}$ chosen to represent the Bloch waves. The number of such $\vec{G}_\parallel$ will be called N. When (2.2) is inserted in Schrödinger's equation, the result is a set of N coupled one-dimensional equations,

$$\left(\frac{d^2}{dz^2}+2E-|\vec{k}_\parallel-\vec{G}_\parallel|^2-2V_0(z)\right)u_{\vec{G}_\parallel}(z)$$

$$=2\sum_{\vec{G}'_\parallel\neq\vec{G}} V_{\vec{G}_\parallel-\vec{G}'_\parallel}(z)u_{\vec{G}'_\parallel}(z)\,. \tag{2.3}$$

The energy E in (2.3) is that of the Bloch waves obtained in the first step of the calculation.

We wish to solve Schrödinger's equation in the surface region using step-by-step integration. This method appears to offer computational efficiency. It also avoids the difficulties present in variational calculations for scattering problems, which are inherently nonlinear.[13] To use step-by-step integration, however, we must have starting values, and these must be based on the boundary conditions. Finding the means to satisfy the boundary conditions and start the integration proves to be the most difficult part of the wave-function calculation.

For discussion of this and related points, we will introduce the following notation: $U(z)$ will be an N-component-column vector whose components are the $u_{\vec{G}_\parallel}(z)$ introduced in (2.2), in some particular order. $\Psi(z)$ will be the incident Bloch wave in the same representation. Each of its components is the sum of $\psi_{\vec{G}}e^{i(k_z-G_z)z}$ for all $\vec{G}$ which have the same $\vec{G}_\parallel$. $\Psi'(z)$ will be the corresponding vector for the reflected Bloch wave.

The *a priori* over-all boundary conditions on the wave function are the requirements that it reduce to the asymptotic forms previously discussed. Thus the wave function must decay into the vacuum,

$$U(z)\to 0 \quad \text{as } z\to+\infty\,. \tag{2.4}$$

The numerically integrated wave functions must match a linear combination of the incident and reflected waves in value and slope at the plane $z=z_M$ which defines the surface region. Therefore,

$$U(z_M)=e^{-i\varphi/2}\Psi(z_M)+e^{i\varphi/2}\Psi'(z_M)\,, \tag{2.5}$$

$$\left.\frac{dU}{dz}\right|_{z_M}=e^{-i\varphi/2}\left.\frac{d\Psi}{dz}\right|_{z_M}+e^{i\varphi/2}\left.\frac{d\Psi'}{dz}\right|_{z_M}\,, \tag{2.6}$$

where φ is the one-dimensional scattering phase shift (yet to be determined), and the coefficient of the incident wave has been chosen to make the wave function real.

The coupled equations (2.3) require $2N$ constants to uniquely determine their solution. However, the conditions (2.4)–(2.6) constitute $3N$ equations, and introduce only one additional constant φ, so that the problem as formulated is overdetermined. What has been omitted is the fact that Schrödinger's equation for the bulk potential admits $N-1$ additional solutions which have the same E, the same $\vec{k}_\parallel$, and which decay exponentially to the left. These "evanescent waves" could be included on the right-hand side in (2.5) and (2.6), and would introduce just the needed number of additional coefficients. However, to include these waves is not

consistent with our intention in distinguishing two regions as we have. The evanescent waves are generated by the physical surface—not by the matching plane. If the matching plane is chosen so that the potential to its left equals that of the bulk to the desired accuracy, self-consistency demands that the wave functions must have already reached their asymptotic limit to a comparable degree of accuracy.

The way to obtain a mathematically well-determined set of conditions without the evanescent waves is to replace (2.6) with the requirement that the mean-squared slope mismatch, which can be represented as the squared magnitude of a complex vector,

$$E_M = \left| e^{-i\varphi/2}\frac{d\Psi}{dz} + e^{i\varphi/2}\frac{d\Psi'}{dz} - \frac{dU}{dz}\right|^2_{z_M}, \qquad (2.7)$$

be minimized. E_M is the kinetic energy arising from the slope mismatch, so our condition can be viewed as an energy-variational principle. This type of approximation is well known in band-structure calculations, since it occurs in Slater's augmented-plane-wave method.[14] In that context, the slope mismatch occurs between the sets of basis functions used inside and outside spheres surrounding each atom, and it is minimized in the calculation. In our calculation, we monitor the mismatch, and have the option of moving the matching plane deeper into the bulk if it should become unacceptably large.

The task of determining starting values for the numerical integration is still not a simple one. Boundary values are specified on both the right- and the left-hand side, and those on the left-hand side implicitly depend on the result of the integration. To carry out the integration, we introduce a mesh of points $z_1, z_2, \ldots, z_M$ with uniform spacing h starting well into the vacuum and ending at the matching plane. The integration algorithm which we use is discussed in detail in the Appendix. For the present discussion we need only observe that the integration from z_n to z_{n+1} can be expressed as a stepping matrix S_n operating on a column vector Y_n representing the wave function,

$$Y_{n+1} = S_n Y_n . \qquad (2.8)$$

The algorithm requires that Y_n contain values of the wave function at four adjacent points. It is thus a $4N$-component vector formed by interleaving the vectors U_n, U_{n-1}, U_{n-2}, and U_{n-3}. The nature of the algorithm is such that the Y_n contains accurate values of U for the points $n-1$, $n-2$, and $n-3$, but only a preliminary estimate for the point n. We will need an $N\times 4N$ matrix Q which picks the leftmost accurate U out of Y,

$$U_n = QY_{n+1} . \qquad (2.9)$$

The simplest boundary condition to satisfy is that referring to the vacuum (2.4). We choose the starting point for the integration far enough out that for $z_1 > z > z_4$, the potential $V_{\vec{G}_\parallel}(z)$ can be neglected for $|\vec{G}_\parallel| \neq 0$, and adequately represented by a constant plus a decaying exponential for $|\vec{G}_\parallel| = 0$. The set of differential equations is then decoupled in this region, and can be solved analytically.[15] Choosing the appropriate decaying solution, the ratios of the components of U_2, U_3, and U_4 to those of U_1 are computed. Using these ratios, we can construct a vector Y_4 for any vector U_1, and represent this process as matrix multiplication by the $4N\times N$ matrix P,

$$Y_4 = PU_1 . \qquad (2.10)$$

With the matrix notation we have established, the process of finding the phase shift and starting values can be explained quite simply. For any set of vacuum starting values U_1, the wave function which satisfies the vacuum boundary condition can be found by a series of matrix multiplications:

$$U_n = Q\left(\prod_{j=4}^{n} S_j\right)PU_1 \equiv T_n U_1 . \qquad (2.11)$$

We can clearly calculate the matrix T_n without reference to any particular U_1. Initially, we calculate T_{M-1} and T_M by the indicated multiplications. Then for any phase shift we can find the U_1 which will cause the amplitude-matching condition (2.5) to be satisfied by inverting T_M,

$$U_1 = T_M^{-1}(e^{-i\varphi/2}\Psi_M + e^{i\varphi/2}\Psi'_M) . \qquad (2.12)$$

In computing the form to be minimized to achieve optimal slope match, the derivatives of Ψ, Ψ', and U are computed from the differences at points M and $M-1$. Nothing is gained from a more sophisticated approximation as long as the same approximation is used for all functions. The form so computed is

$$E_m = h^{-2}\left| e^{-i\varphi/2}(\Psi_{M-1} - T_{M-1}T_M^{-1}\Psi_M) + e^{i\varphi/2}(\Psi'_{M-1} - T_{M-1}T_M^{-1}\Psi'_M)\right|^2 . \qquad (2.13)$$

Varying φ to minimize (2.13), we find

$$\varphi = \mathrm{Im}\ln[(\Psi'_{M-1} - T_{M-1}T_M^{-1}\Psi'_M)^\dagger \times(\Psi_{M-1} - T_{M-1}T_M^{-1}\Psi_M)] . \qquad (2.14)$$

Using this result, we apply (2.12) and (2.11) to compute the wave function for the whole mesh.

Computer code to implement this procedure has been developed and tested. Over-all numerical stability seems excellent, which may be ascertained by comparing both sides of (2.5) at the end of the calculation. With a surface region corresponding to a few atomic layers, slope mismatch

is typically less than 1%. It appears that the transition from the coordinate representation in the surface region to the expansion based on a finite set of z-direction plane waves in the bulk is typically a more serious source of error than the neglect of the evanescent tails.

To compute the valence-charge density in the surface region, the squared amplitude of the wave function must be computed as a function of the incident wave vector, and integrated over the occupied portion of the half of the Brillouin zone with $k_z > 0$. This integral is, of course, approximated by a sum on a finite mesh, and symmetry is used as much as possible to reduce the portion of the zone which must be considered. The symmetry is less than that of the bulk, and portions of the zone which are equivalent in the bulk but have different k_z's give different contributions to the surface-region charge density.

III. POTENTIAL CALCULATION

The potential seen by a valence electron consists of a term from the positive-ion cores and a self-consistent potential due to the other valence electrons. The latter potential is made up of a Hartree term, obtainable exactly from Poisson's equation, and an exchange and correlation term, which we will assume can be expressed as an energy-independent local function of position. One's ability ity to treat the exchange and correlation potential in such a manner has been extensively discussed in the literature[16] and we have nothing further to add on this point.

In treating the ion-core potential we shall replace the exact ion-core-electron interaction by a model potential which is both energy independent and a local function of position. The success of the empirical pseudopotential has been amply demonstrated[11] for calculating bulk properties, and the principle of pseudoatom transferability in the area of compound semiconductors and liquid metals has received strong empirical support. We believe the same transferability is valid between atoms in the bulk and those in the surface.

In light of the above assumptions we may write the potential energy as seen by an electron in the surface region as

$$V(\vec{x}) = V_H(\vec{x}) + V_{x-c}(\vec{x}) + V_{\text{ion}}(\vec{x}) , \tag{3.1}$$

where $V_H(\vec{x})$ is the Hartree potential, $V_{x-c}(\vec{x})$ is the exchange and correlation potential caused by the valence charge, and $V_{\text{ion}}(\vec{x})$ is a model pseudopotential for the electron-ion interaction. We shall discuss each of these terms in considerable detail below.

The Hartree potential $V_H(\vec{x})$ satisfies the equation

$$\nabla^2 V_H(\vec{x}) = -4\pi\rho(\vec{x}) , \tag{3.2}$$

where $\rho(\vec{x})$ is the electron density and we have adopted atomic units. This equation is easily solved by Fourier transformation parallel to the surface. Writing

$$V_H(\vec{x}) = \sum_{\vec{G}_\parallel} e^{i\vec{G}_\parallel \cdot \vec{x}_\parallel} V^H_{\vec{G}_\parallel}(z) , \tag{3.3a}$$

$$\rho(\vec{x}) = \sum_{\vec{G}_\parallel} e^{i\vec{G}_\parallel \cdot \vec{x}_\parallel} \rho_{\vec{G}_\parallel}(z) , \tag{3.3b}$$

and substituting (3.3) into (3.2) one obtains

$$\left(G_\parallel^2 - \frac{d^2}{dz^2}\right) V^H_{\vec{G}_\parallel}(z) = 4\pi\rho_{G_\parallel}(z) , \tag{3.4}$$

where $G_\parallel = |\vec{G}_\parallel|$ and we have suppressed the vector notation because of the dependence of $V^H_{G_\parallel}(z)$ and $\rho_{G_\parallel}(z)$ on only $|\vec{G}_\parallel|$.

The solution to (3.4) is best discussed separately for the cases $G_\parallel = 0$ and $G_\parallel \neq 0$. For $G_\parallel = 0$, (3.4) takes the form

$$-\frac{d^2}{dz^2} V_0^H(z) = 4\pi\rho_0(z) . \tag{3.5}$$

We are interested in solving (3.5) to the right of the matching plane (see Fig. 1) subject to the following boundary conditions on the plane:

$$V_0^H(z_M) = V_0 , \tag{3.6a}$$

$$\frac{dV_0^H}{dz}(z_M) = 0 , \tag{3.6b}$$

where the constant V_0 is adjusted to assure continuity. These conditions are appropriate when the matching plane is chosen as in Fig. 1 as a center of inversion symmetry for the planar average bulk potential.

While equation (3.5) subject to boundary conditions (3.6) constitutes a routine numerical problem, a number of points are worth mentioning in connection with its solution. First, our knowledge of $\rho_0(z)$ will be restricted to a discrete set of equispaced points in the surface region, i.e., the set used in Sec. II to solve the Schrödinger equation. These are the same points at which we will want to know V_0^H. The total integrated valence charge density is fixed by the number of atom layers in the surface region and their valency. In general the $\rho_0(z)$ calculated from the Schrödinger equation, which serves as input to (3.5), will not have precisely the correct total amount of charge. In order to ensure proper charge neutrality we would like to scale $\rho_0(z)$. This is particularly important at the initial stages of the iteration towards self-consistency. Close to self-consistency we expect the charge to be very close to its correct value with little or no scaling required. This scaling can be done in the process of solving (3.5). Substituting $W = dV_0^H/dz$ into (3.5), one obtains

$$-\frac{dW(z)}{dz}=4\pi\rho_0(z)\,, \tag{3.7a}$$

$$W(z_m)=0\,. \tag{3.7b}$$

We can solve (3.7) by step-by-step numerical integration using quadratic interpolation for $\rho_0(z)$. We now scale the resulting $W(z)$ uniformly so that

$$W(z_\infty)=-4\pi Q_T\,,$$

where z_∞ is a point sufficiently far into the vacuum that the approximation $\rho(z_\infty)=0$ is valid (z_4 of Sec. II), and Q_T is the total positive charge per unit area residing on the ion cores in the surface region. Using the scaled $W(z)$ in

$$\frac{dV_0^H}{dz}=W(z)\,, \tag{3.8a}$$

$$V_0^H(z_m)=V_0\,, \tag{3.8b}$$

one can again integrate numerically to obtain a $V_0^H(z)$ consistent with charge neutrality.

Turning to the case of $G_\parallel\neq 0$, we can best solve (3.4) by Green's functions. One finds

$$V_{G_\parallel}^H(z)=\frac{2\pi}{G_\parallel}\int_{z_m}^{\infty}\rho_{G_\parallel}(z')\,e^{-G_\parallel|z-z'|}\,dz' + A_{G_\parallel}e^{-G_\parallel(z-z_m)}\,, \tag{3.9}$$

where we have added to the particular solution of the inhomogeneous Eq. (3.4) a solution of the homogeneous equation. The potential $V_{G_\parallel}^H(z)$ satisfies the physical requirement of exponential decay into the vacuum, and depending on $A_{G_\parallel}$ can assume any value at $z=z_m$. Given (3.9) a simple algorithm can be used to generate $V_{G_\parallel}^H$ from a knowledge of $\rho_{G_\parallel}$ at an equidistinct set of points.

The exchange and correlation potential $V_{x\text{-}c}(\vec{\mathbf{x}})$ can be handled with comparative simplicity as long as we make the local density approximation. Since the aim of this paper is largely exploratory we adopt the simplest "reasonable" form for the exchange and correlation potential,[16]

$$V_{x\text{-}c}(\vec{\mathbf{x}})=F[\rho(\vec{\mathbf{x}})]^{1/3}\,. \tag{3.10}$$

This form has ample historical precedent in self-consistent band calculations, and with the added flexibility of having F adjustable can be used to achieve close agreement over a limited density range between (3.10) and more complicated local expressions for exchange and correlation, such as the Wigner interpolation formula.[16] The question then arises as to the validity of (3.10) in the vacuum region where the density has dropped considerably from its bulk value. There is no question that (3.10) ceases to be valid in the tail of the electron density. Fortunately, the uncertainties in the form of the potential far into the vacuum have very little feedback on the charge density—even in the vacuum region. This is because these uncertainties are quite small when referenced to the Fermi energy and cause only small changes in the way the individual wave functions tail into the vacuum. Having discussed our choice for the exchange and correlation potential we turn to the more technical question of how we obtain $V_{G_\parallel}^{x\text{-}c}(z)$ from $\rho_{G_\parallel}(z)$. The direct approach would be Fourier synthesis of $\rho_{G_\parallel}(z)$ to obtain $\rho(\vec{\mathbf{x}})$, the calculation of $\rho^{1/3}(\vec{\mathbf{x}})$, and then its subsequent Fourier decomposition. While this method is direct it can be very time consuming. What one would like is an analytic procedure from which one can obtain $V_{G_\parallel}^{x\text{-}c}(z)$ directly from $\rho_{G_\parallel}(z)$. Such a procedure is easily obtained for the $\rho^{1/3}$ choice for exchange and correlation. In that case

$$V_{x\text{-}c}=F[\rho_0(z)+\sum_{\vec{G}_\parallel}\rho_{G_\parallel}(z)\,e^{i\vec{G}_\parallel\cdot\vec{\mathbf{x}}_\parallel}]^{1/3} \tag{3.11}$$

and

$$V_{x\text{-}c}=F\rho_0(z)^{1/3}\,[1+\sum_{\vec{G}_\parallel}\bar{\rho}_{G_\parallel}(z)\,e^{i\vec{G}_\parallel\cdot\vec{\mathbf{x}}_\parallel}]^{1/3}\,, \tag{3.12}$$

where

$$\bar{\rho}_{G_\parallel}(z)=\rho_{G_\parallel}(z)/\rho_0(z)\,. \tag{3.13}$$

What we require at this point is an efficient polynomial expansion of $(1+y)^{1/3}$. In the case of nearly-free-electron metals, where $\rho(\vec{\mathbf{x}})$ does not vary by more than 50% in the bulk, a Taylor expansion of $(1+y)^{1/3}$ is rapidly convergent. For example,

$$(1+y)^{1/3}=1+1/3y-1/9y^2\,,\quad |y|\leq 0.3 \tag{3.14}$$

has a maximum error of 0.2% over that entire range. Using (3.14) in (3.12) it is a trivial matter in this case to collect terms and obtain directly $V_{G_\parallel}^{x\text{-}c}(z)$. By way of illustration (from our calculation for sodium), if we retain two nonzero $|\vec{G}_\parallel|$'s one finds

$$V_0^{x\text{-}c}(z)=F\rho_0(z)^{1/3}\,[1-\tfrac{4}{9}\,(\bar{\rho}_{G_1}(z)^2+\bar{\rho}_{G_2}(z)^2)]\,, \tag{3.15a}$$

$$V_{G_1}^{x\text{-}c}(z)=F\rho_0(z)^{1/3}\{\tfrac{1}{3}\,\bar{\rho}_{G_1}(z)[1-\tfrac{2}{3}\,\bar{\rho}_{G_2}(z)]\}\,, \tag{3.15b}$$

$$V_{G_2}^{x\text{-}c}(z)=F\rho_0(z)^{1/3}\,[\tfrac{1}{3}\,\bar{\rho}_{G_2}(z)-\tfrac{2}{9}\,\bar{\rho}_{G_1}(z)^2]\,. \tag{3.15c}$$

In the case where the charge density varies greatly, as in semiconductors, the same type of procedure can be used except that a Chebyshev approximation to $(1+y)^{1/3}$ must be used instead of a Taylor expansion to achieve an efficient polynomial representation.[17]

As previously stated, we are going to use a model pseudopotential to describe the ion-core potential. Perhaps the simplest of these is the Ashcroft model potential.[18] It combines the advantages of great simplicity, extensive use, and reasonable success when applied to the s-p-bounded

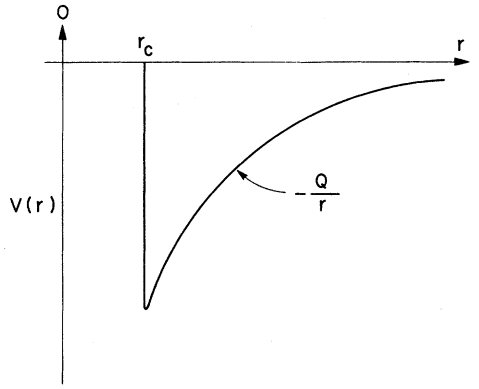

FIG. 2. Radial dependence of the Ashcroft model potential for an isolated ion. The potential is zero inside the core radius r_c and Coulombic outside.

metals. This potential is shown schematically for the pseudoion in Fig. 2. The potential is Coulombic outside a radius R_c and zero inside. It can be thought of as being generated by a repulsive core,

$$V_{\text{core}}(\vec{x}) = Q/R_c\,, \quad |\vec{x}| \le R_c$$
$$= 0\,, \quad |\vec{x}| > R_c \tag{3.16}$$

where Q is the valence charge on the atom, and a shell of positive charge Q distributed on the surface of a sphere with radius R_c.

The Fourier transform of the core potential is easily obtained in closed form. For the body-centered lattice it is

$$V_{G_\parallel}^{\text{core}}(z) = \sum_n \frac{2\pi}{a^2 G_\parallel}\,[r_c^2 - (z - z_n)^2]^{1/2} \times J_1(G_\parallel[r_c^2 - (z - z_n)^2]^{1/2}) \times \Theta(r_c^2 - (z - z_n)^2)\, e^{i(\vec{G}_\parallel \cdot \vec{b})n}\,, \tag{3.17}$$

where a is the lattice constant of the body-centered-cubic lattice, z_n is the position of the core centers projected onto the z axis, J_1 is the first-order Bessel function, and $\vec{b} = \frac{1}{2}(a, a, 0)$. The function $\Theta(z)$ is 1 for $z > 0$ and 0 otherwise. A close examination of the exponential term indicates that it depends only on $G_\parallel$ and simply produces alternations is the sign of $V_{G_\parallel}^{\text{core}}(z)$ between adjacent cores for those $G_\parallel$ for which $|(a/2\pi)\vec{G}_\parallel|^2$ is an odd integer.

For calculating the Coulomb potential from the core charge all we need is the Fourier transform of the core charge,

$$\rho_{G_\parallel}^{\text{ion}}(z) = \frac{eQ}{2r_c a^2} \sum_n J_0(G_\parallel[r_c^2 - (z - z_n)^2]^{1/2}) \times \Theta(r_c^2 - (z - z_n)^2)\, e^{i(\vec{G}_\parallel \cdot \vec{b})n}\,. \tag{3.18}$$

This can be inserted into Poisson's equation (3.4) and the resulting potential obtained just as was done for the electron charge density.

Until now we have concentrated mainly on the potential in the surface region. This is because we shall be assuming that the potential in the bulk is known from empirical pseudopotential calculations. There is still the question of consistency between the potential generated in the surface region and that adopted in the bulk. This problem is handled at two levels. First, having the bulk pseudopotential at a limited number of reciprocal-lattice vectors we can generate a mixed or Laue representation for the bulk potential,

$$V_B(\vec{x}) = \sum_{\vec{G}_1} V_{\vec{G}}^B\, e^{i\vec{G}\cdot\vec{x}} = \sum_{\vec{G}_\parallel} e^{i\vec{G}_\parallel \cdot \vec{x}_\parallel}\, V_{\vec{G}_\parallel}^B(z)\,, \tag{3.19}$$

where

$$V_{\vec{G}_\parallel}^B(z) = \sum_{G_z} e^{iG_z z}\, V_{\vec{G}_\parallel, G_z}^B\,. \tag{3.20}$$

Continuity between $V_{\vec{G}_\parallel}^B(z)$ and $V_{\vec{G}_\parallel}(z)$ at the surface plane can then be assured with the help of the adjustable constants V_0 and $A_{\vec{G}_\parallel}$ which enter in solving Poisson's equation. While this assures continuity of the potential across the matching plane, unless the model potential in the surface region is chosen to be reasonably consistent with the bulk pseudopotential, the shape of $V_{\vec{G}_\parallel}(z)$ on either side of the matching plane will be very different.

The detailed means one uses to bring about at least partial consistency will vary depending on the kind of solid one is dealing with. For the case of sodium the following procedure, which should be valid for all materials with weak pseudopotentials, was used. The self-consistent pseudopotential in the bulk was calculated using a dielectric function consistent with our assumed form for exchange and correlation in the surface region.[19] This leads to the following relation between the pseudopotential coefficients and the model potential:

$$V_G^B = \left(V_G^{\text{core}} - \frac{4\pi}{G^2}\,\rho_G^{\text{core}}\right) \Bigg/ \left\{1 + \frac{f(G/2k_F)}{\pi k_F} \times \left[\frac{4k_F^2}{G^2} + F\left(\frac{\pi}{3}\right)^{1/3}\right]\right\}\,, \tag{3.21}$$

where

$$f(x) = \tfrac{1}{2} + \frac{1 - x^2}{4x} \ln\left|\frac{1 + x}{1 - x}\right|\,. \tag{3.22}$$

One then chooses a core radius R_c to give a best fit to the empirical pseudopotential[20] parameter. Once R_c is chosen, the V_G^B's generated from (3.21) are used in the bulk calculation. By this means potentials for the bulk and surface region are generated which are highly consistent with each other.

IV. APPLICATION TO Na

In order to examine the practical applicability of our method to real materials we have carried it out for the (100) surface of Na. We considered

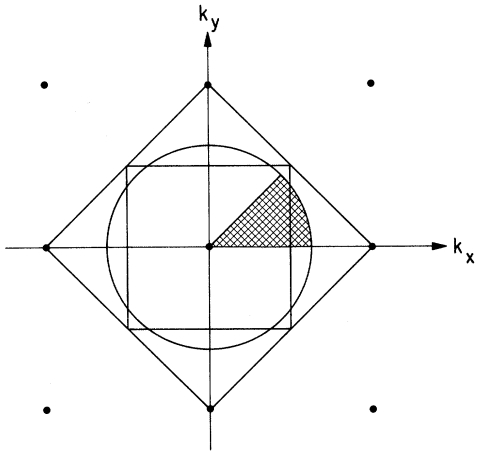

FIG. 3. Surface reciprocal lattice for the (100) face of Na. The interior square is the surface Brillouin zone, and the outer square is the projection of the bulk Brillouin zone. The circle is the projection of the Fermi surface, and the shaded octant indicates the set of incident wave vectors used in the charge-density integration.

this a good first choice for two reasons. First, bulk Na is known to be well described by a weak pseudopotential and to have a nearly spherical Fermi surface.[11] Second, this surface has been studied by Kohn and Lang using a perturbation scheme for the lattice potential, and they found that the work function was changed significantly by the inclusion of the lattice.[4]

Bulk Na is a bcc metal with lattice constant 8.091 a.u. and Wigner-Seitz radius $r_s = 3.99$ a.u. The atoms on the (100) surface form a simple square lattice. The surface projection of the reciprocal lattice is a simple square mesh. One could define an associated surface Brillouin zone which is shown in Fig. 3. It should be noted that this is not the same as the projection of the three-dimensional Brillouin zone onto the surface, which is also shown in Fig. 3. While the Fermi surface is completely inside the first bulk Brillouin zone, its projection overlaps the boundaries of the surface Brillouin zone. There is no discontinuous behavior of the wave functions we calculate at the surface Brillouin-zone boundary. However, we note that an attempt to solve the coupled differential equations (2.3) perturbationally would break down near this boundary.

The symmetry of the terminated lattice is such that one need only consider incident Bloch states whose wave vector lies in a one-eighth section of the Fermi hemisphere, the projection of which is shown in Fig. 3. For a $\vec{k}$ in this section, the most important bulk reciprocal-lattice vectors in the secular equation are (0, 0, 0), (1, 0, 1), (0, 1, 1), and (1, 1, 0). These $\vec{G}$'s, projected onto the surface plane, give a set of $\vec{G}_{\parallel}$'s consisting of (00), (10), (01), and (11).

Initial experience with this set revealed sizeable slope discontinuities at the matching plane. We found that this resulted from the fact that our wave functions in the surface region had their z dependence calculated, in principle, in complete detail, while the bulk wave functions each had only a single z-direction Fourier component. We found this problem could be rectified by adding bulk $\vec{G}$'s to give additional Fourier components in the z direction. Our final set included, in addition to the previously mentioned four, (0, 0, ± 2), (1, 1, ± 2), (1, 0, − 1), and (0, 1, − 1). With this expanded set, we are no longer calculating the bulk wave function in a symmetric fashion, and we might be tempted to include more $\vec{G}$'s such as (2, 0, 0). This, however, would introduce another $\vec{G}_{\parallel}$, and to avoid slope-mismatch problems with this component, even more $\vec{G}$'s seem unavoidable. When the basis set is sufficiently enlarged to yield convergence for the band structure, this asymmetry will have no effect.

Another difficulty with our restricted initial selection of $\vec{G}$'s is that while for $\vec{k}$'s near the Fermi surface they clearly dominate other $\vec{G}$'s in the wave function, for small $\vec{k}$'s other $\vec{G}$'s are almost as important. Our approximation causes us to underestimate the $\vec{G}_{\parallel} \neq 0$ components of the charge density. As a crude but plausible means of correcting this defect, we have calculated weighting factors for each point in the $\vec{k}$-integration mesh used to calculate the charge density. These factors were chosen so that the contribution to each component of the bulk charge density from each k point calculated with the restricted basis would agree with the perturbation-theory result from the full basis.

The k integration was carried out in cylindrical coordinates, with point positions and weighting factors chosen by a product of appropriate Gauss-Jordan quadrature formulas.[21] Two different mesh sizes were employed to verify convergence, one containing 24 points and the other 30 points (equivalent to 240 points in the complete Fermi hemisphere).

The Ashcroft model potential for Na was fit to the bulk empirical pseudopotential $V_{110} = 0.079$ by choosing a core radius of 1.6. (All numbers quoted are in a.u. unless otherwise specified.) This is somewhat different from the radius of 1.67 originally calculated by Ashcroft[18] because we have taken account of the exchange-correlation correction to the screening in the Slater approximation. The ions were positioned maintaining the bulk lattice spacing all the way to the surface, although this is not demanded by the method. Means of calculating surface relaxation are discussed in

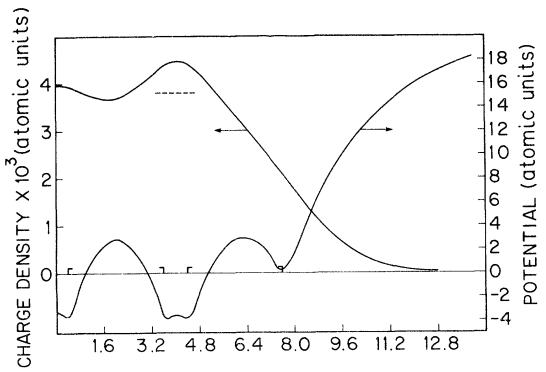

FIG. 4. Charge density (left axis) and self-consistent potential (right axis) averaged over the x-y plane as a function of z. The two pairs of small brackets along the abscissa indicate the positions of the ion cores of the last two atomic layers. Note that right axis scale is 10^{-2} a.u.

Sec. V.

Self-consistent calculations were carried out with two and with three atomic layers in the surface region. A mesh-point spacing of 0.4 was used in the numerical integration, and the first mesh point was 7.2 into the vacuum beyond the outermost point of the last layer of cores.

To begin the calculation, we guess a physically reasonable charge distribution in the surface region. The distribution is the product of the bulk charge density found from linear-response theory times a function which cuts off smoothly as it passes into the vacuum, $1\text{-}\tanh\beta(z - z_0)$. z_0 is placed at the equivalent jellium edge, and β is adjusted to reproduce the surface dipole found in the appropriate jellium calculation.[4] This charge distribution is used to calculate a starting approximation to the potential by the methods described in Sec. III.

The potential was made the center of attention in the iterative convergence scheme. The components $V_{G_\parallel}(z)$ with $G_\parallel \neq 0$ converged quickly and stably using simple iteration. This was not the case for $V_0(z)$, since this component is an extremely sensitive function of the electron distribution. For example, an input potential with a work function slightly below the converged result yielded after a single cycle of iteration an output potential with a work function considerably too large. Thus the "feedback" is so strong that simple iteration is completely unstable. We dealt with this problem by the standard technique of constructing a new input $V_0(z)$ by adding $(1 - \alpha)$ times the previous input V_0 to α times the corresponding output V_0. We found that an α of around 0.1 critically damped the instability. On the last few iterations, we increased α to as much as 0.4. This ensured convergence of those details of the potential which do not feed back too strongly on themselves. We terminated these iterations before the unstable features could run away. An average of 6–9 runs was adequate to obtain convergence to 1%. This entire procedure required 2 min of computing time on a Honeywell 635 computer.

In discussing the results of the calculation, let us first consider the $G_\parallel = 0$ components of the potential and charge density. These are shown in Fig. 4 for the case in which two atomic layers were included in the surface region. We first note that the potential of the next-to-last atomic layer is very similar to that of the bulk. Only in the last layer does the rising surface barrier distort the bulk potential. Outside the last core, the potential rises rather quickly, but then slows its rise and finally approaches its vacuum asymptote of 0.213 rather slowly. The charge density rises smoothly from zero in the vacuum to a peak midway between the first and second atomic layers. In the bulk, one would expect a peak at this location whose height was 6% above the average due to the lattice potential. The peak we find here is 14% above the average, and the enhancement is due to the first Friedel oscillation. Examination of the jellium calculation shows that this oscillation occurs at the same location and has an amplitude of 8%.[4] Thus the two effects appear to superpose linearly.

In order to display the three-dimensional behavior of the potential, we have plotted it on the cross-hatched plane shown in Fig. 5. In this sketch, representing an outermost unit cell of the solid, atoms 1 and 2 lie, respectively, in the first and second layers. The left-hand edge of the cross-hatched plane is its intersection with the matching plane in the two-layer calculation. In Fig. 6, the

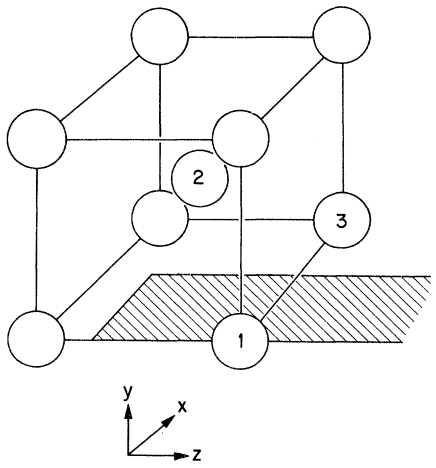

FIG. 5. Sketch of a unit cell containing the surface layer (atoms 1 and 3) and the next layer (atom 2). The cross-hatched plane is the location of the plot shown in Fig. 6.

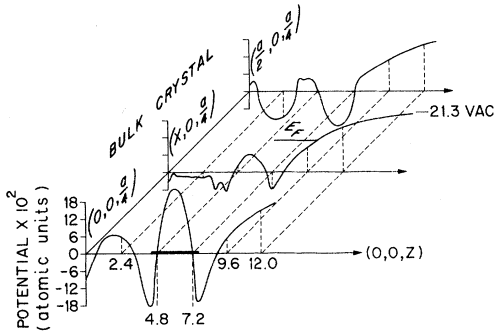

FIG. 6. Three-dimensional self-consistent potential for the Na (100) surface. The potential is plotted vertically along three lines in the cross-hatched plane shown in Fig. 5, whose proportions have been distorted for clarity. The location of the core of the atom labeled 1 in Fig. 5 is indicated by the heavy line along the foreground abscissa, and the left boundary is the matching plane.

potential is plotted along three equally spaced lines lying in the cross-hatched plane, whose proportions have been distorted for clarity. The prominent peak in the foreground is the repulsive core potential of the atom labeled 1. A marked difference can be seen in the rate at which the vacuum barrier rises as one passes from a position just outside atom 1 to one midway between atoms 1 and 3. Quantatively, the effective electric field in the plane 1 Å outside the cores varies from 3.3 to 1.4 V/Å as one moves between these two positions. Another indication of the strength of the three-dimensional structure in the potential is the fact that a 0.4-eV variation in its value exists over the plane 2 Å outside the cores. Inside the first atomic layer, the structure of the potential is essentially equivalent to that of the bulk.

The work function is the difference between the vacuum potential and the Fermi energy. Because of the known near-sphericity of the Na Fermi surface and nearly-free-electron band mass, we calculated ϵ_F simply by finding the lowering of the band minimum relative to the bulk average potential (which is our zero reference), and assuming free-electron dispersion. We find 2.71 eV for the work function. This is to be compared with a value of 3.06 eV found by Kohn and Lang for the jellium model and with their perturbation-theory estimate for the (100) Na face of 2.75 eV.[4] We consider this result and ours to be essentially in agreement. Experimental data is available only for polycrystalline samples, for which a value of 2.7 eV is found.[22] Since crystal-face anisotropy of the work function is usually portional to the packing density of the face,[5] and since the (100) face is an intermediate density face, it is plausible that its work function be nearly equal to the polycrystalline average.

V. DISCUSSION OF FURTHER APPLICATIONS

As in any elaborate self-consistent calculation, computing time requirements place an upper bound on the complexity of the systems that can be studied. The gratifyingly short time requirements of our Na calculation suggest that the method should be useful without modification for a fairly large number of materials and surfaces.

The chief factor entering into the determination of the computing time is the number of $\vec{G}_{\parallel}$ wave vectors which are needed in the wave-function calculation. As the number N of $\vec{G}_{\parallel}$'s increases, the most time-consuming step is ultimately the series of matrix multiplications needed to construct the matrices T_M and T_{M-1} for the phase-shift determination. The time required for this operation increases as N^3. We believe that the set of $\vec{G}_{\parallel}$'s which are necessary for the accurate determination of the phase shift will generally be considerably smaller than the set we wish to include to get an accurate representation for charge density. In order to exploit this situation, we have devised a perturbational scheme for integrating the less-important equations in (2.3) after our nonperturbational procedure is applied to the main components. Computation time for this only increases linearly with the number of $\vec{G}_{\parallel}$'s beyond the basic set.

So far we have only discussed scattering states, but the possibility exists that some systems we wish to treat will have true bound surface states which lie in a gap of the bulk crystal and decay exponentially into the bulk.[1] The method we have described can be adapted quite easily to calculate such states. Only for an energy equal to the eigenvalue will a wave function integrated from the vacuum into the bulk be strictly decaying. If, for a given $\vec{k}_{\parallel}$, the amplitude of a wave function at the matching plane which was started at a fixed amplitude in the vacuum displays a sharp minimum as a function of energy, we conclude a bound state exists at the energy of the minimum. The actual calculation is slightly more involved because of the multicomponent nature of the wave function. The vector U_1 which is the eigenvector of $\tilde{T}_M T_M$ with the smallest eigenvalue $\lambda_0(\vec{k}_{\parallel}, E)$ gives the best set of starting values, and λ_0 itself is then the squared amplitude at the matching plane. This method is clearly practical only for identifying states that are sufficiently strongly bound to be well localized within the surface region.

With the techniques already developed and the extensions outlined above, our methods should be applicable to all s-p–bonded systems amenable to pseudopotential treatment. This class includes nontransition metals and semiconductors. It also includes ordered adsorbed layers which are commensurate with the underlying lattice.

A quantity of considerable interest beyond the electronic structure itself is the surface energy. The total energy of a system is the sum of the one-electron energies minus the electron-electron interaction plus the ion-ion interaction. The change in the one-electron energies produced by the formation of the surface can be obtained directly from the phase shift introduced in Sec. II and the bulk E-vs-$\vec{k}$ relation. The interaction energies in the surface region can be found directly from the calculated potentials and charge densities. Since all of these quantities are already calculated in the course of determining the electronic structure, calculation of the surface energy requires a negligible amount of additional computer time.

Up to this point we have not discussed the manner in which the positions of the ion planes in the surface region should be chosen. While for the Na calcalation we simply used the bulk spacing, there is nothing in the method that requires this. The spacing should, in fact, be determined to minimize the surface energy. Doing so will enable us to study the interesting phenomenon of surface relaxation and to find the equilibrium spacing of ordered adsorbed layers. The energy can also be studied as the last layer is rigidly slid around parallel to the substrate to determine preferred bonding sites.

The method we have introduced, including the extensions discussed in this section, appears to be useful for the study of surface properties of a wide variety of materials. An important class of materials to which the method is not directly applicable is transition metals and their compounds. Studies of means of extending the scheme to these cases are currently underway.

APPENDIX: DIFFERENTIAL-EQUATION INTEGRATION SCHEME

The cross coupling of the set of differential equations (2.3) presents a special problem. The second derivative $u''_{G_\parallel}$ at mesh point n depends on the values of all the $u_{G_\parallel}$ at that point. This rules out the accurate Numerov scheme which is popular in atomic and band calculations.[23] However, an equally accurate two-step ("predictor-corrector") scheme due to Milne can be used.[24] Its general form for the equation

$$\frac{d^2y}{dx^2}=f(x,y) \tag{A1}$$

is the predictor

$$y_{n+1}=y_n+y_{n-2}-y_{n-3}+1/4h^2(5f_n+2f_{n-1}+5f_{n-2}) , \tag{A2}$$

followed by the corrector

$$y_n=2y_{n-1}-y_{n-2}+1/12h^2(f_n+10f_{n-1}+f_{n-2}) , \tag{A3}$$

where y_j and f_j refer to the jth mesh point. In principle, (A2) is used once and (A3) is iterated to consistency using the predicted value to compute f_n on the first iteration. In practice, we have found that a single application of (A3) yields very accurate and stable results.

In the following, we will use integer superscripts to refer to $\vec{G}_\parallel$ wave vectors and subscripts to denote mesh points. The $4N$ component vector Y in (2.8) is

$$Y_n=\begin{bmatrix} u_n^1 \\ u_{n-1}^1 \\ u_{n-2}^1 \\ u_{n-3}^1 \\ u_n^2 \\ \vdots \\ u_{n-3}^N \end{bmatrix} . \tag{A4}$$

The $4N\times 4N$ stepping matrix S_n in (2.8) is

$$S_n=\begin{bmatrix} S_n^{11} & S_n^{12} & \cdots & S_n^{1N} \\ S_n^{21} & S_n^{22} & \cdots & S_n^{2N} \\ & \vdots & & \\ S_n^{N1} & S_n^{N2} & \cdots & S_n^{NN} \end{bmatrix} , \tag{A5}$$

where the indicated elements are each 4×4 submatrices. The factors on the left-hand side in the differential equation (2.3) are denoted by an effective wave vector squared for each component,

$$(\kappa_n^i)^2=|\vec{k}_\parallel-\vec{G}_\parallel^i|^2+2V_0(z_n)-2E . \tag{A6}$$

Then the diagonal submatrices are

$$S_n^{ii}=\begin{bmatrix} 1+\frac{5}{4}h^2\kappa_n^i & \frac{1}{2}h^2\kappa_{n-1}^i & 1+\frac{5}{4}h^2\kappa_{n-2}^i & -1 \\ \frac{1}{12}h^2\kappa_n^i & 2+\frac{5}{6}h^2\kappa_{n-1}^i & -1+\frac{1}{12}h^2\kappa_{n-2}^i & 0 \\ 0 & 1 & 0 & 0 \\ 0 & 0 & 1 & 0 \end{bmatrix} . \tag{A7}$$

The off-diagonal submatrices are

$$S_n^{ij}=\begin{bmatrix} \frac{5}{4}h^2V_n^{ij} & \frac{1}{2}h^2V_{n-1}^{ij} & \frac{5}{4}h^2V_{n-2}^{ij} & 0 \\ \frac{1}{12}h^2V_n^{ij} & \frac{5}{6}h^2V_{n-2}^{ij} & \frac{1}{12}h^2V_{n-2}^{ij} & 0 \\ 0 & 0 & 0 & 0 \\ 0 & 0 & 0 & 0 \end{bmatrix} , \tag{A8}$$

where V_n^{ij} is $V_{\vec{K}}(z_n)$; $\vec{K}=\vec{G}_\parallel^i-\vec{G}_\parallel^j$. The top two rows in each submatrix implement the algorithm, and the last rows of the diagonal submatrices simply move already computed values down in the Y vector. Note that components of Y_n referring to the

nth point are "predicted" values, while those referring to the preceding three points are "corrected" values.

The $N\times 4N$ matrix Q introduced in (2.9) has all zero elements except

$$Q_{n,4n-2}=1\ . \tag{A9}$$

The decoupled differential equations in the vacuum have the form

$$\left(\frac{d^2}{dz^2}-(\kappa^i)^2+\alpha^2 e^{-\lambda z}\right)u^i(z)=0\ , \tag{A10}$$

where κ is the limit of (A6) for $z\to+\infty$, and $\frac{1}{2}\alpha^2$ and λ are the amplitude and decay rate of the exponential tail of the $\vec{G}_{\parallel}=0$ component of the potential. The desired solution is[15]

$$u^i(z)=J_{2\kappa/\lambda}[(2\alpha/\lambda)e^{-\lambda z/2}]\ , \tag{A11}$$

where J is a Bessel function. The ratios

$$r_j^i=u^i(z_j)/u^i(z_1) \tag{A12}$$

are computed, and the $4N\times N$ matrix P introduced in (2.10) is given by

$$P=\begin{bmatrix} r_4^1 & 0 & \\ r_3^1 & 0 & \\ r_2^1 & 0 & \\ 1 & 0 & \\ 0 & r_4^2 & \\ 0 & r_3^2 & \\ 0 & r_2^2 & \cdot \\ 0 & 1 & \cdot \\ 0 & 0 & \cdot \\ \cdot & \cdot & 0 \\ \cdot & \cdot & r_4^N \\ \cdot & \cdot & r_3^N \\ & & r_2^N \\ & & 1 \end{bmatrix}\ . \tag{A13}$$

[1]S. G. Davison and J. D. Levine, in *Solid State Physics*, edited by H. Ehrenreich, F. Seitz, and D. Turnbull (Academic, New York, 1970), Vol. 25.

[2]D. W. Jepsen, P. M. Marcus, and F. Jona, Phys. Rev. Letters 26, 1365 (1971).

[3]J. Bardeen, Phys. Rev. 49, 653 (1936); J. R. Smith, *ibid.* 181, 522 (1969); A. J. Bennett and C. B. Duke, *ibid.* 160, 541 (1967).

[4]N. D. Lang, Solid State Commun. 7, 1047 (1969); N. D. Lang and W. Kohn, Phys. Rev. B 1, 4555 (1970); 3, 1215 (1971).

[5]R. Smoluchowski, Phys. Rev. 60, 661 (1941).

[6]C. F. von Weizäcker, Z. Physik 96, 431 (1935).

[7]J. R. Smith, Phys. Rev. Letters 25, 1023 (1970).

[8]A. J. Bennett and C. B. Duke, Phys. Rev. 188, 1060 (1969).

[9]D. S. Boudreux, Phys. Rev. B 1, 4551 (1970).

[10]A preliminary report of this work was presented at the 32nd Annual Conference on Physical Electronics, 1972, Albuquerque, New Mexico, Sandia Laboratories (unpublished).

[11]See *Solid State Physics*, edited by H. Ehrenreich, F. Seitz, and D. Turnbull (Academic, New York, 1970), Vol. 24.

[12]M. von Laue, Phys. Rev. 37, 53 (1931); P. M. Marcus and D. W. Jepsen, Phys. Rev. Letters 20, 925 (1968).

[13]P. M. Morse and H. Feshbach, *Methods of Theoretical Physics* (McGraw-Hill, New York, 1953), p. 1703.

[14]J. C. Slater, Phys. Rev. 51, 846 (1937).

[15]D. J. BenDaniel and C. B. Duke, Phys. Rev. 152, 683 (1966).

[16]J. C. Slater, Phys. Rev. 81, 385 (1951); W. Kohn and L. J. Sham, *ibid.* 140, A1133 (1965); E. P. Wigner, *ibid.* 46, 1002 (1934).

[17]L. Fox, *Numerical Solution of Ordinary and Partial Differential Equations* (Addison-Wesley, Reading, Mass., 1962).

[18]N. W. Ashcroft, Phys. Letters 23, 48 (1966).

[19]A. W. Overhauser, Phys. Rev. B 3, 1888 (1971).

[20]This is the precise procedure used by Ashcroft (Ref. 18) except he ignored exchange and correlation.

[21]G. Szego, *Orthogonal Polynomials* (American Mathematical Society, New York, 1959).

[22]R. L. Gerlach and T. N. Rhodin, Surface Sci. 19, 403 (1970).

[23]F. Herman and S. Skillman, *Atomic Structure Calculations* (Prentice-Hall, Englewood Cliffs, N. J., 1963).

[24]W. E. Milne, *Numerical Calculus* (Princeton U. P., Princeton, N. J., 1949), p. 140.